Section: Neurosystems
Associate Editor: Laszlo Acsady

# Hippocmpal CA3 and CA2 have distinct bilateral innervation patterns to CA1 in rodents

Yoshiaki Shinohara[1], Aki Hosoya[1], Kazuko Yahagi[1], Alex S. Ferecskó[2], Kunio Yaguchi[3], Attila Sík[2], Makoto Itakura[4], Masami Takahashi[4], and Hajime Hirase[1,5*]

1. Laboratory for Neuron Glia Circuit
RIKEN Brain Science Institute
Wako 351-0198, Japan

2. Neuronal Networks Group
College of Medical & Dental Sciences
School of Clinical & Experimental Medicine,
University of Birmingham, United Kingdom
Birmingham, B15 2TT, United Kingdom

3. Laboratory for Behavioral Genetics
RIKEN Brain Science Institute
Wako 351-0198, Japan

4. Kitasato University School of Medicine
Department of Biochemistry
Sagamihara 228-8555, Japan

5. Saitama University Brain Science Institute
Saitama 338-8570, Japan

Running Title: Rodent hippocampal CA3 and CA2 projection to CA1

Number of pages: 24
Number of figures: 7
Number of tables: 2
Number of words: Whole manuscript (4767), Abstract (234) Introduction (520), Discussion (1217)

* To whom correspondence should be addressed
Hajime Hirase
RIKEN Brain Science Institute (BSI)
Wako-shi, 351-0198, Japan
Tel +81-48-462-1111 x 7474
Fax +81-48-467-6918
hirase@brain.riken.jp

## Abstract

Ipsi- and contralateral hippocampal CA3-CA1 and CA2-CA1 projections were investigated in adult male Long-Evans rats by retrograde tracing. Injection of the retrograde tracer cholera toxin subunit B in the *strata oriens* and *radiatum* of dorsal CA1 resulted in labeling of predominantly pyramidal cells in ipsi- and contralateral CA3 and CA2. The anterior-posterior extent of CA3 innervation to CA1 was similar in contralateral and ipsilateral. Fifteen to twenty percent of the hippocampus proper cells that gives rise to CA1 *stratum oriens* innervation were represented by CA2 pyramidal cells, whereas CA2 cells represented a mere three percent for CA1 *stratum radiatum* innervation. The preferred projection of CA2 pyramidal cells to the CA1 *stratum oriens* is also manifested in transgenic mice that express GFP under the control of the CACNG5 promoter, in which CA2 cells express high amounts of GFP. The ratio of ipsilateral versus contralateral projection was compared. For the CA3-CA1 connection, we found that dorsal CA1 *stratum radiatum* received more ipsilateral projections whereas CA1 *stratum oriens* received more contralateral innervation. Interestingly, ipsilateral connections dominated for both CA2-CA1 *stratum oriens* and CA2-CA1 *stratum radiatum*. These results demonstrate that the primary intrahippocampal target of CA2 pyramidal cells is the ipsilateral CA1 *stratum oriens*, which is distinct from CA3 cells that project more diversely to bilateral CA1 regions. Such innervation patterns may hint to a differential dendritic information processing in apical and basal dendrites of CA1 pyramidal cells.

## Introduction

The hippocampus is a brain structure critically involved in the formation of episodic memory. In rodents, the left and right hippocampi are interconnected (Blackstad, 1956) with functional synapses (Andersen *et al.*, 1966), suggesting a cooperation of left and right hippocampi in information processing. Two major commissural projection systems have been described in the rodent hippocampus. The molecular layer of the dentate gyrus receives projections from the contralateral hilar cells (Hjorth-Simonsen & Laurberg, 1977; Fricke & Cowan, 1978; Laurberg, 1979; West *et al.*, 1979). The hilar cells that gives rise to the commissural projections are found to be widespread in the septo-temporal axis except for a small portion in the temporal end (Laurberg & Sorensen, 1981) by use of the extended hippocampal preparation (Gaarskjaer, 1978). In addition, CA3 pyramidal cells give rise to commissural projections to CA3 and CA1 (Hjorth-Simonsen, 1973; Swanson *et al.*, 1978; Laurberg & Sorensen, 1981). In fact, a single CA3 pyramidal cell can project both ipsi- and contralaterally (Swanson *et al.*, 1980) and extend their axons to as much as 75% of the septo-temporal extent of CA1 in both sides (Tamamaki *et al.*, 1984; Li *et al.*, 1994). Moreover, the CA3-CA1 commissural axons terminate in the *stratum oriens* and the *stratum radiatum* (Andersen *et al.*, 1966; Buzsaki & Eidelberg, 1982) and make synapses on both pyramidal cells (Andersen *et al.*, 1966; Gottlieb & Cowan, 1972) and non-pyramidal neurons (Frotscher & Zimmer, 1983). Although the existence of these projections has been described previously, the bilateral connectivity of CA3-CA1 has not been systematically studied.

Additionally, the projection from CA2, a small region between CA3 and CA1 that lacks *stratum lucidum*, has received much scattered attention. Yet, mounting evidence suggests that the CA2 region forms a functional cluster. For example, using acutely prepared hippocampal slices, a voltage sensitive dye imaging study demonstrated that CA2 relays some CA3 input to CA1 (Sekino *et al.*, 1997) and electrophysiological studies showed that CA2 receives strong input from the entorhinal cortex (EC) (Bartesaghi & Gessi, 2004; Chevaleyre & Siegelbaum, 2010). One of the reasons that CA2 escaped from detailed descriptive studies is possibly because of its narrow area and vague definition. Recent genetic mapping of mouse brain regions by the Allen

Brain Atlas project has proposed renewed definitions of CA2 (Lein *et al.*, 2005). The voltage dependent calcium channel gamma subunit 5 (CACNG5, also known as TARP gamma-5) is a molecule that regulates specific AMPA receptor conductances and highly expressed in CA2 (Fukaya *et al.*, 2005; Kato *et al.*, 2008) and cerebellum (Fukaya *et al.*, 2005; Soto *et al.*, 2009).

In this study, we addressed four fundamental questions on CA3-CA1 and CA2-CA1 commissural connections of rodent hippocampus using cholera toxin subunit B (CTB) as a retrograde tracer and CACNG5 to visualize the molecularly defined CA2 region: (1) What is the proportion of ipsi- to contralateral input conversing to the CA1 *strata oriens* and *radiatum*? (2) Does the commissural connectivity change along the anterior-posterior axis? (3) Does CA2 region, the region between CA3 and CA1 project to the contralateral CA1? (4) What are the proportions of CA3 and CA2 inputs in different layers of CA1?

## Material and methods

The procedures involving animal care, surgery and sample preparation were approved by the Animal Experimental Committee of RIKEN Brain Science Institute and performed in accordance with the guidelines of the Animal Experimental Committee of RIKEN Brain Science Institute.

### Subjects and Surgery

Twenty-eight adult (> postnatal 2 months old) male Long-Evans rats were anesthetized with ketamine-xylazine cocktail (9% w/v ketamine and 1% xylazine in 0.9% NaCl, dosage: 1.0 ml/kg) and rigidly fixed in a stereotaxic apparatus. A small craniotomy was made at the stereotaxic coordinate indicated in Table 1. A filamented glass capillary (Kwik-Fil, WPI) of tip diameter ~20 μm was filled with cholera toxin subunit B (CTB) conjugated with Alexa Fluor 488 (C34775, Invitrogen, 1 μg/μl in PBS). The glass capillary was mounted to a fine mechanical manipulator (Model 961, Kopf) and slowly lowered to the designated depth from the surface of the brain. Fluorescent tracers were iontophoretically injected by passing a positive current of 5 μA (7 s on, 7 s off) for 30 minutes using a stimulus isolator (A360, WPI). In some experiments, local

field potential was monitored through the CTB containing electrode to navigate the electrode to the targeted layer. Upon the electrode arrival at the target, the electrode connection was switched from the preamplifier to the stimulus isolator by a mechanical toggle switch. This strategy was particularly useful when targeting to posterior hippocampus, as the intense pyramidal cell firing at the entry to the *stratum pyramidale* can be used as a reliable reference. After iontophoresis, the capillary was slowly withdrawn and the incision was sutured. Antibiotic ointment (Gentacin ointment, Schering-Plough) was topically applied at the suture.

## Histology

### CTB immunohistochemistry

Five to seven days after CTB microinjection, the rats were deeply anesthetized with urethane (i.p., dosage 1.9 g/kg). Transcardiac perfusion was performed with 200 ml saline (0.9% NaCl solution), followed by 250 ml 4% paraformaldehyde in 0.1 M phosphate buffer (PB). The brain was removed and postfixed for at least three hours in the fixative solution. Coronal sections of thickness 60 μm were prepared in PB using a microslicer (Pro-7 Linear Slicer, DSK, Japan). After washing in Tris buffered saline (TBS) and blocking background immunoreactivity in 3% bovine serum albumin for at least 45 minutes in room temperature, the sections were incubated with in TBS containing 0.3% Triton X-100 and a combination of antibodies against AlexaFluor 488 (1:1000, A11094, Molecular Probes) and CTB (1:1000, ab34992, Abcam) for overnight or longer in 4 °C while gently shaking. The sections were then washed three times in TBS and incubated in biotinylated secondary antibody against rabbit IgG (1:300 in TBS, 01821-04, Nacalai Tesque, Japan). The biotin signal was amplified with the ABC Elite Kit (1:400, Vector Laboratories), and was subsequently developed using DAB-Ni as the chromogen. Six consecutive sections were mounted per slide glass using gelatin. After drying in room temperature, the sections were counterstained with cresyl violet.

### CACNG5 antibody

The antibody against CACNG5 was raised in the guinea pig using the synthetic peptide CSSDASLQMNSNYPAL, conjugated with keyhole limpet hemocyanin. After immunization, the antiserum was purified by affinity column conjugated with the peptide. The specificity of antibody was tested by performing Western blot analysis

using mouse cerebral cortex and cerebellum homogenates (10µg protein each) with an antibody concentration of 0.5µg/ml, which yielded a distinguished band at ~31 kDa in the cerebellar, but not cerebral cortical sample.

#### CACNG5 immunostaining

Eight week-old rats were deeply anesthetized with urethane and transcardially perfused with 200 ml saline, followed by 250 ml 2% paraformaldehyde in 0.1 M PB. The brain was removed, post-fixed in the same fixative for overnight, and coronal sections of thickness 60 µm were prepared. The sections were blocked for 2 hours with TBS supplemented with 2% normal goat serum and 0.1 % Triton X-100. The sections were then incubated in TBS with the CACNG5 antibody (1:500 guinea pig). For CA2 definition in Fig. 2, three consecutive sections from a rat were incubated with the antibody for CACNG5, calbindin-D28k (1:1000 rabbit CB-38a, Swant), and striatal enriched tyrosine phosphatase (STEP) (1:2000, mouse, Novus Biologicals, Littleton, CO). The sections were incubated in primary antibodies for two days at 4 °C. Signals were detected by biotinylated secondary antibody and ABC Elite Kit as described above.

#### GFP immunohistochemistry

The polyclonal rabbit antibody used for immunohistochemical detection of GFP was described previously (Tomioka & Rockland, 2006). The antibody was used at a dilution of 1:1500 and applied solely or in combination with the CACNG5 antibody to characterize the GFP expression pattern of the CACNG5-GFP transgenic mice (see below). Immunoreactivity was detected by fluorescent secondary antibodies (Alexa 488) or DAB-Ni, as described above.

## Generation of Transgenic mice

The BAC transgenic construct containing the mouse CACNG5 gene with IRES-GFP (GENSAT1-BX1300) was obtained from the BAC PAC Resources hosted by the Children's Hospital Oakland Research Institute via GENSAT (Gong *et al.*, 2003). Microinjections of the transgenic construct into the pronuclei of C57BL/6-fertilized embryos generated eight transgenic lines, of which a line (#475) that had a prominent GFP expression in CA2 cells was used. Transgenic mice were genotyped by polymerase

chain reaction with primer pairs targeted to GFP. Mice that were approximately postnatal two months old were sacrificed for immunohistochemical studies.

### Data Analysis

All of the developed sections (90~100 sections per rat) covering the entire hippocampus were subject to cell-counting and examined using a standard light microscope (BX51, Olympus). Pyramidal cells were identified based on their morphology and cell body location in the *stratum pyramidale*, as marked by cresyl violet staining. Cells were counted manually under brightfield microscopy using 40x or 20x objective lens. Only cell bodies with diameter larger than ten micrometer were counted. A set of CACNG5 immunostained coronal sections covering the entire hippocampal formation was prepared to build a reference sample to delineate the CA2 region (see Results). Cell counts were recorded for each brain section, and the cell counts within the same slide glass (i.e. from six consecutive brain sections) were summed up and used for further statistics. To calculate the proportion of the CA3 or CA2 cells projecting to a dye-injected area in CA1, the cell counts for each slide glass was divided by the total cell counts of the ipsi-lateral (i.e. dye-injected) side. Measured and computed values are represented as mean ± standard error of the mean, and statistical comparisons were made with the Wilcoxon test, unless otherwise indicated.

## Results

### Retrograde tracing by CTB

Iontophoretic injections of the retrograde tracer CTB were performed in various locations of hippocampal CA1. Total of 28 injection experiments are analyzed. The injection sites included the anterior CA1 *stratum radiatum* (n = 3 + 3 animals; left-injected + right-injected), the anterior CA1 *stratum oriens* (n = 3 + 4), the posterior CA1 *stratum radiatum* (n = 5 + 3), and the posterior CA1 *stratum oriens* (n = 3 + 4). The stereotaxic coordinates of the injection sites are described in Table 1. Dye injection sites were identified by the appearance of intense neuropil labeling (Fig. 1A). The area of intense labeling typically spanned 150-250 μm in radius (see Suppl. Fig. 1 for a more detailed examination of injection sites). Both ipsi- and contralateral CA3 pyramidal

cells were retrogradely labeled (Fig. 1A-C). While CA3 pyramidal cell labeling was dominant, cells with non-pyramidal morphology were also occasionally labeled outside the CA3 *stratum pyramidale*, confirming the existence of contralaterally projecting non-pyramidal cells reported previously (Schwerdtfeger & Buhl, 1986; Zappone & Sloviter, 2001). These putative interneurons were excluded from the current analyses. The distribution of the retrogradely labeled cells usually covered a wide range along the longitudinal (anterior-posterior) axis (Fig. 1D,E).

In addition to CA3 pyramidal cells, CA2 pyramidal cells were also labeled by CTB. To distinguish the CA2 region from CA3, we first sacrificed a rat and performed immunohistochemistry against CACNG5, and built a reference sample that defines the CA2 region. The CACNG5 antibody was raised as described in the methods section and the specificity of the antibody was assessed first by performing Western blot using mouse brain homogenate. We demonstrated that a band at ~31 kDa is clearly visible in the cerebellar homogenate but not in the cerebral cortical homogenate (Fig. 2A). Next, immunohistochemistry using the antibody in a rat cerebellar section showed a distinct localization of the target molecule in Bergmann glia (Fig. 2B). Both results are in agreement with the previous reports of CACNG5 distribution in the brain. The CA2 areas marked by CACNG5 and STEP immunohistochemistry appeared compatible (Fig. 2C). The molecularly defined CA2 area was broader than the classical definition of CA2 (i.e. the large cell body region that lacks *stratum lucidum*, Fig. 2C). At an anterior-posterior coordinate of ~-4.3 mm, the CA3a portion occupied about one third of the molecularly defined CA2. Moreover, a large dorsal portion of the cell body layer of an anterior coronal section (-2.1 mm from the bregma, Fig. 2D) was demarcated by CACNG5 immunohistochemistry, whereas a narrow region between CA3 and CA1 was labeled in a more posterior section (-4.3 mm from the bregma, Fig. 2D). Using this reference, we counted retrogradely labeled CA2 and CA3 pyramidal cells in 60 μm coronal sections (Fig. 2D). The total number of retrogradely traced cells varied from animal to animal due to subtle differences of the electrode tip diameter or the electrode series resistance resulting in varied injected tracer volume. On average, we counted 1883 ± 385 and 14477 ± 1794 CTB-labeled cells per animal in CA2 and CA3, respectively.

## Ipsilateral *vs.* Contralateral CA3-CA1 projection

In anterior CA1, innervations to the *stratum oriens* or *stratum radiatum* originated preferentially from the anterior portion of CA3 (Fig. 3, left panels). Projections from the anterior one third of CA3 accounted for 65 ± 2% in the CA1 *stratum oriens* and 66 ± 5% in the CA1 *stratum radiatum* (ipsi- and contralateral projections combined). Projections from the posterior one third of CA3 accounted for only 5 ± 1% in the CA1 *stratum oriens* and 4 ± 1% in the CA1 *stratum radiatum*. There are substantial differences in the contra- *vs.* ipsilateral connection ratio (CIR) between CA3-CA1 *stratum oriens* and CA3-CA1 *stratum radiatum* projections. In the anterior CA1 *stratum oriens*, the CIRs were 1.21 ± 0.11, 2.13 ± 0.25, 2.65 ± 0.46 in the anterior, middle, and posterior one third of coronal sectioning of CA3, respectively, indicating that the contralateral projection dominated over the ipsilateral projection. By contrast, ipsilateral projection was dominant in the CA1 *stratum radiatum* (CIR: 0.54 ± 0.04, 0.68 ± 0.04, 1.01 ± 0.16 for the anterior, middle, and posterior one third of CA3).

The posterior CA1 *stratum oriens* received projections from a widespread portion of CA3 with slightly more retrogradely labeled cells in the central portion of CA3 (Fig. 3, right panels). A similar tendency was observed for CA3 projections to the posterior CA1 *stratum radiatum* with a more evenly-spread distribution. The relative contributions of ipsi- and contralateral innervation in *strata oriens* and *radiatum* appeared similar to that of anterior CA1. The posterior CA1 *stratum oriens* was preferentially innervated by contralateral CA3 (CIR: 1.36 ± 0.11, 1.31 ± 0.12, 2.10 ± 0.22, for the anterior, middle, and posterior one third of CA3). By contrast, the posterior CA1 *stratum radiatum* was preferentially innervated by ipsilateral CA3 (CIR: 0.24 ± 0.02, 0.42 ± 0.03, 0.59 ± 0.08 for the anterior, middle, and posterior one third of CA3).

## Ipsilateral vs. Contralateral CA2-CA1 projection

Similar analyses were made on the CA2-CA1 projection (Fig. 4). Unlike the CA3-CA1 projection, the vast majority of CA2 pyramidal cell axons projecting to anterior CA1 originated from the anterior one third (CA1 *stratum oriens*: 99 ± 0.1%, CA1 *stratum radiatum* 99 ± 0.3%). The CIRs of anterior CA2 to the CA1 *stratum oriens* and the CA1 *stratum radiatum* projections were 0.36 ± 0.04 and 0.08 ± 0.01,

respectively. The majority of CA2 pyramidal cell axons to posterior CA1 originated from the anterior (CA1 *stratum oriens*: 51 ± 2%, CA1 *stratum radiatum*: 51 ± 2%) and middle (CA1 *stratum oriens*: 66 ± 4%, CA1 *stratum radiatum*: 34 ± 4%) CA2. The CIRs of anterior CA2 to the CA1 *stratum oriens* and the CA1 *stratum radiatum* projections were 0.66 ± 0.05 and 0.10 ± 0.02, respectively. The CIRs of mid CA2 to the CA1 *stratum oriens* and CA1 *stratum radiatum* projections were 0.40 ± 0.05 and 0.08 ± 0.02, respectively.

Overall, we found that contralateral projection is dominant for CA3 projections to the CA1 *stratum oriens* (CIR: 1.45 ± 0.13 for anterior CA1, 1.42 ± 0.11 for posterior CA1, Fig. 5A). By contrast, ipsilateral projection was dominant for CA3 projections to the CA1 *stratum radiatum* (0.61 ± 0.02 for anterior CA1, 0.41 ± 0.03 for posterior CA1). The ipsilateral and contralateral innervation balance of CA2-CA1 projection was characteristically different from that of CA3-CA1 projection (Fig. 5B). Namely, ipsilateral innervation dominated for both *stratum oriens* (CIR: 0.36 ± 0.04 for anterior CA1, 0.52 ± 0.03 for posterior CA1) and *stratum radiatum* (CIR: 0.09 ± 0.01 for anterior CA1, 0.09 ± 0.12 for posterior CA1). Despite the general ipsilateral dominance of CA2-CA1 projection, the proportion of contralateral projection to CA1 *stratum oriens* was higher than that to CA1 *stratum radiatum*, as it was the case for the CA3-CA1 projection.

## CA3 vs. CA2 projection ratio to CA1

We computed the relative contributions of CA3 and CA2 projections to CA1 (Fig. 5C). The contribution of CA2 input to CA1 was generally modest in the *stratum oriens* (15~20%) and very small in the *stratum radiatum* (< 4%). More precisely, the relative contribution is summarized in Table 2. The CA3:CA2 input ratio appeared similar between the anterior and posterior CA1 *stratum oriens* ($P = 0.16$, Wilcoxon test on the CA2/CA3 contribution ratio). Likewise, the CA3:CA2 input ratio was similar between the anterior and posterior CA1 *stratum radiatum* ($P \approx 1.00$, Wilcoxon test on the CA2/CA3 contribution ratio). These results suggest that there is a uniform organization of CA3:CA2 input ratio throughout the anterior-posterior axis.

## CA2 innervation target within CA1

From the retrograde tracing experiments in rats, it was difficult to determine the ratio of CA2 innervations to CA1 *strata oriens* and *radiatum*. Therefore, we utilized a transgenic mouse line (#475) that expresses GFP under the control of the CACNG5 promoter. GFP expression was seen in a narrow region between CA1 and CA3 that colocalized with CACNG5 expression (Fig. 6A). Visualizing CA3 *stratum lucidum* by calbindin-D28k immunostaining in dorsal hippocampus revealed that the GFP expressing region overlapped with some ~120 μm of the distal portion of CA3a (Fig. 6B), consistent with the immunohistochemical result in the rat (Fig. 2). Indeed, the proximal end of the GFP expressing cell population appears to be where the mossy fiber projection starts to taper off. Interestingly, the proportion of CA3a region in the molecularly defined GFP expressing CA2 area progressively increased in posterior part of the hippocampus (Fig. 6C).

Immunohistochemistry against GFP revealed intense labeling of CA2 pyramidal cells and faint labeling of a sparse population of CA1 pyramidal neurons (Fig. 7A). In addition to the cell bodies and dendrites of CA2 pyramidal cells, the CA1 *strata oriens* and *radiatum* were labeled in a pattern that resembled axonal morphology (Fig. 7B). In this transgenic mouse line, neurons in the habenula, lateral septum, thalamus and intercalated nuclei of amygdala also expressed visible amounts of GFP (not shown). Among these regions, the nucleus reuniens of the thalamus sends axonal projections to the CA1 *stratum lacunosum-moleculare* (Wouterlood *et al.*, 1990; Dolleman-Van der Weel & Witter, 2000), but none of the other regions are known to project to CA1. Therefore, the axon-like labeling in CA1 *strata oriens* and *radiatum* likely represents axons from the CA2 pyramidal cells. Magnified views of *strata oriens* and *radiatum* using a 100x objective (N.A. 1.30) show that the *stratum oriens* is more intensely labeled than the *stratum radiatum* (Fig. 7B,C). Furthermore, the most intense labeling was seen in the inner part of *stratum oriens* (i.e. the region closer to *stratum pyramidale*) and the immunoreactivity was weaker in the *alveus* end of the *stratum oriens* forming presumably an axon innervation gradient. These results suggest that CA2 innervations to CA1 occur both in the *strata oriens* and *radiatum*, with a preference to the *stratum* oriens, in particular the region close to the *stratum pyramidale*.

Moreover, distal CA1 (i.e. closer to the subiculum) was more intensely labeled with GFP than the proximal CA1 (i.e. closer to CA2/CA3).

## Discussion

The hippocampus is one of the most intensively investigated part of the brain due to its critical role in formation of episodic memory for humans and spatial memory for rodents. Hence, the anatomy of the hippocampus, in particular the trisynaptic loop (EC-DG-CA3-CA1), has been rigorously studied since the beginning of the twentieth century (for instance, Ramón y Cajal (1911)). Many of the anatomical studies are focused on the ipsilateral connections of rodent hippocampus (Witter & Amaral, 2004; Amaral & Lavenex, 2007), presumably because of the overwhelming popularity of electrophysiological experiments that use rodent hippocampal slices. In rodents, however, the hippocampi in both hemispheres are heavily interconnected. One of the main commissural projections arises from CA3 pyramidal cells and terminates in CA1. Although the existence of the commissural projection has been long-recognized, a systematic and quantitative description of bilateral CA3-CA2 and CA3-CA1 projections with statistical evaluation has not been performed to the authors' knowledge. Using CTB as a retrograde tracer, we investigated intra-hippocampal pyramidal cell projections to CA1 of Long-Evans rats, one of the most popular rat strains used in spatial memory behavioral experiments. We systematically described the relative contribution of ipsi- and contralateral projections from CA3 and CA2 to CA1. As a result, we found that CA3 and CA2 have distinct projection patterns to CA1.

The anatomical definition of CA2 is the region between CA1 and CA3 that has large pyramidal cells and does not receive mossy fiber innervation (i.e. no *stratum lucidum*). While this classical definition of CA2 is still respected, molecular definitions of the CA2 region have become popular and widely accepted (Lein *et al.*, 2005). Amongst the well-known molecules that delineates CA2 from other hippocampal regions are fibroblast growth factor 2 (FGF2), adenosine A1 receptor, alpha-actinin 2, STEP, and CACNG5 (Williams *et al.*, 1996; Wyszynski *et al.*, 1997; Ochiishi *et al.*, 1999; Zhao *et al.*, 2007; Kato *et al.*, 2008). Moreover, the Allen Brain Atlas project has suggested a multiple number of genes that characterize different CA regions as well as

dorsal and ventral hippocampal areas (Lein *et al.*, 2004; Lein *et al.*, 2005; Lein *et al.*, 2007; Thompson *et al.*, 2008). Many of the molecular definitions of CA2 include a minor portion of CA3a cells, which may be linked to the functional dynamics of the hippocampus. For instance, CA2 and CA3a is innervated by the supramammillary body (Stanfield & Cowan, 1984; Magloczky *et al.*, 1994), which are implicated in generating theta rhythms (Vertes & McKenna, 2000). In particular, we find that for both STEP and CACNG5, the proximal border of CA2 is at the point where the *stratum lucidum* start to taper off. These observations suggest that the CA3a region within the molecularly defined CA2 is where anatomical transition occurs in terms of mossy fiber innervation.

We chose CACNG5 as a CA2 marker as our antibody had a reasonable immunohistochemical pattern in paraformadehyde fixed rat hippocampal sections and also CACNG5 has a significant role in AMPA receptor function in CA2 pyramidal cells (Kato *et al.*, 2008). As in Fig. 2 and 7, the region CACNG5 is largely compatible with another widely accepted CA2 marker protein STEP. The visualization of a specific marker for the CA2 region allowed us to count individually retrogradely-labeled CA2 cells. As a result, we saw the distinct innervation patterns of CA2 pyramidal cells to CA1.

Previous studies using *in vivo* intracellular dye injections reported that CA2 pyramidal cells extend their axons to the CA1 *stratum oriens*, but not to *stratum radiatum* (Ishizuka *et al.*, 1990; Ishizuka *et al.*, 1995), while other studies using *in vivo* or *in vitro* intracellular dye injection suggest that CA2 pyramidal cells innervate to both the *strata oriens* and *radiatum* (Tamamaki *et al.*, 1988; Mercer *et al.*, 2007). Our results agree with the latter, as we find that CA2 cells can be retrogradely traced from both CA1 *strata oriens* and *radiatum*, although the proportion of innervation was smaller in the *stratum radiatum*. A previous study reported that the axon arborization of a single CA2 pyramidal cell covers the entire dorsal extent of the hippocampus (Tamamaki *et al.*, 1988). Our study further suggests that CA2 pyramidal cell arborizations tend to have an axon density gradient that peaks at a similar anterior-posterior location of CA1. On this note, the CA3 cells that project to a CA1 region are more broadly distributed with a mild peak at a similar anterior-posterior position as the target CA1 position. Such ipsi-

and contralateral connection patterns are in agreement with an electrophysiological study that systematically showed ipsi- and contralaterally evoked local field potential responses to CA3 stimulation (Finnerty & Jefferys, 1993).

Our results demonstrate that CA2 cells projects to both ipsi- and contralateral CA1, as supported by previous single cell tracing and viral tracing studies (Tamamaki *et al.*, 1988; Sik *et al.*, 2006). However, we find that the CA2-CA1 *stratum oriens* and CA2-CA1 *stratum radiatum* projections are heavily biased to be ipsilateral with the ipsilateral fibers representing approximately 70% and 90% of the respective CA2-CA1 projections. By contrast, CA3-CA1 *stratum oriens* projection is dominated by the contralateral projection, and the contralateral projection represent approximately 60%. The CA3-CA1 *stratum radiatum* projection is between 60% and 70% ipsilateral connections. Physiological studies have indicated that CA2 forms a distinct functional module within the trisynaptic loop. For example, CA2 pyramidal cells receive strong input from the entorhinal cortex (Bartesaghi & Gessi, 2004; Chevaleyre & Siegelbaum, 2010), while receiving somewhat weaker synaptic inputs from CA3 (Chevaleyre & Siegelbaum, 2010). Moreover, CA3-CA2 synapses was shown to be somewhat harder to be potentiated than CA3-CA1 synapses (Zhao *et al.*, 2007). Interestingly, CA2-CA1 synapses were recently been reported to be functionally strong (Chevaleyre & Siegelbaum, 2010). Our observation that CA2 axons preferentially terminate in the region of the *stratum oriens* closer to the *stratum pyramidale*, may provide a mechanism for the strong synaptic inputs from CA2 pyramidal cells.

From our retrograde tracing experiments, it was not possible to determine statistically significant differences between left and right contralateral projections. We combined the left- and right-injected samples equally, as our preliminary result in mice suggests that the ipsilateral CA3-CA1 synapse density in CA1 *stratum radiatum* is not significantly different between the left and right hemispheres (Shinohara *et al.*, 2008). On the other hand, the left and right tissue volume or cell number differences have been reported for rodent hippocampus, although the dominant side varies from study to study (Diamond *et al.*, 1982; Diamond *et al.*, 1983; Verstynen *et al.*, 2001; Lister *et al.*, 2006; Spring *et al.*, 2010). Moreover, glutamate receptor subtypes of CA3-CA1 synapses are

influenced by the lateral origin of the presynaptic neurons in mice (Kawakami *et al.*, 2003; Shinohara *et al.*, 2008; Kohl *et al.*, 2011). Future studies should address if hippocampal projection patterns are also asymmetrically arranged. Such a study may provide a fundamental basis for understanding lateralized hippocampal functions (Burgess *et al.*, 2002, for a review). Finally, the highly significant proportion of contralateral innervation to CA1 in rodents hints at a tight functional coupling of the left and right hippocampi. Interestingly, changes in the expression of spatial learning-related genes first occur in the right hippocampus, whereas engram formation appears to be biased to the left hippocampus (Klur *et al.*, 2009). It is intriguing to speculate that such transfer of cellular activation is mediated by these commissural connections.

## Acknowledgements

This work was supported by RIKEN intramural funding, KAKENHI grants (23115522, 21650081, 21700440, 20500291, 21300141) from the MEXT of Japan, Human Frontiers Science Foundation (RGY0073/2006) and MRC (G1001235), Welcome Trust Travel Fellowship (ASF). We thank Ryohei Tomioka for sharing the GFP antibody, Elizabeth Hur for comments on an earlier version of the manuscript, Mika Tanaka and Shigeyoshi Itohara for help on trasngenic mouse generation, Thomas J. McHugh for help on STEP immunohistochemistry.

## References

Amaral, D. & Lavenex, P. (2007) Hippocampal Neuroanatomy. In Andersen, P., Morris, R., Amaral, D., Bliss, T., O'Keefe, J. (eds.) *The Hippocampus Book*. Oxford University Press, New York, pp. 37-114.

Andersen, P., Blackstad, T.W. & Lomo, T. (1966) Location and identification of excitatory synapses on hippocampal pyramidal cells. *Exp Brain Res*, **1**, 236-248.

Bartesaghi, R. & Gessi, T. (2004) Parallel activation of field CA2 and dentate gyrus by synaptically elicited perforant path volleys. *Hippocampus*, **14**, 948-963.

Blackstad, T.W. (1956) Commissural connections of the hippocampal region in the rat, with special reference to their mode of termination. *J Comp Neurol*, **105**, 417-537.

Burgess, N., Maguire, E.A. & O'Keefe, J. (2002) The human hippocampus and spatial and episodic memory. *Neuron*, **35**, 625-641.

Buzsaki, G. & Eidelberg, E. (1982) Convergence of associational and commissural pathways on CA1 pyramidal cells of the rat hippocampus. *Brain Res*, **237**, 283-295.

Chevaleyre, V. & Siegelbaum, S.A. (2010) Strong CA2 pyramidal neuron synapses define a powerful disynaptic cortico-hippocampal loop. *Neuron*, **66**, 560-572.

Diamond, M.C., Johnson, R.E., Young, D. & Singh, S.S. (1983) Age-related morphologic differences in the rat cerebral cortex and hippocampus: male-female; right-left. *Exp Neurol*, **81**, 1-13.

Diamond, M.C., Murphy, G.M., Jr., Akiyama, K. & Johnson, R.E. (1982) Morphologic hippocampal asymmetry in male and female rats. *Exp Neurol*, **76**, 553-565.

Dolleman-Van der Weel, M.J. & Witter, M.P. (2000) Nucleus reuniens thalami innervates gamma aminobutyric acid positive cells in hippocampal field CA1 of the rat. *Neurosci Lett*, **278**, 145-148.

Finnerty, G.T. & Jefferys, J.G. (1993) Functional connectivity from CA3 to the ipsilateral and contralateral CA1 in the rat dorsal hippocampus. *Neuroscience*, **56**, 101-108.

Fricke, R. & Cowan, W.M. (1978) An autoradiographic study of the commissural and ipsilateral hippocampo-dentate projections in the adult rat. *J Comp Neurol*, **181**, 253-269.

Frotscher, M. & Zimmer, J. (1983) Commissural fibers terminate on non-pyramidal neurons in the guinea pig hippocampus -- a combined Golgi/EM degeneration study. *Brain Res*, **265**, 289-293.

Fukaya, M., Yamazaki, M., Sakimura, K. & Watanabe, M. (2005) Spatial diversity in gene expression for VDCCgamma subunit family in developing and adult mouse brains. *Neurosci Res*, **53**, 376-383.

Gaarskjaer, F.B. (1978) Organization of the mossy fiber system of the rat studied in extended hippocampi. I. Terminal area related to number of granule and pyramidal cells. *J Comp Neurol*, **178**, 49-72.

Gong, S., Zheng, C., Doughty, M.L., Losos, K., Didkovsky, N., Schambra, U.B., Nowak, N.J., Joyner, A., Leblanc, G., Hatten, M.E. & Heintz, N. (2003) A gene expression atlas of the central nervous system based on bacterial artificial chromosomes. *Nature*, **425**, 917-925.

Gottlieb, D.I. & Cowan, W.M. (1972) On the distribution of axonal terminals containing spheroidal and flattened synaptic vesicles in the hippocampus and dentate gyrus of the rat and cat. *Z Zellforsch Mikrosk Anat*, **129**, 413-429.

Hjorth-Simonsen, A. (1973) Some intrinsic connections of the hippocampus in the rat: an experimental analysis. *J Comp Neurol*, **147**, 145-161.

Hjorth-Simonsen, A. & Laurberg, S. (1977) Commissural connections of the dentate area in the rat. *J Comp Neurol*, **174**, 591-606.

Ishizuka, N., Cowan, W.M. & Amaral, D.G. (1995) A quantitative analysis of the dendritic organization of pyramidal cells in the rat hippocampus. *J Comp Neurol*, **362**, 17-45.

Ishizuka, N., Weber, J. & Amaral, D.G. (1990) Organization of intrahippocampal projections originating from CA3 pyramidal cells in the rat. *J Comp Neurol*, **295**, 580-623.

Kato, A.S., Siuda, E.R., Nisenbaum, E.S. & Bredt, D.S. (2008) AMPA receptor subunit-specific regulation by a distinct family of type II TARPs. *Neuron*, **59**, 986-996.

Kawakami, R., Shinohara, Y., Kato, Y., Sugiyama, H., Shigemoto, R. & Ito, I. (2003) Asymmetrical allocation of NMDA receptor epsilon2 subunits in hippocampal circuitry. *Science*, **300**, 990-994.

Klur, S., Muller, C., Pereira de Vasconcelos, A., Ballard, T., Lopez, J., Galani, R., Certa, U. & Cassel, J.C. (2009) Hippocampal-dependent spatial memory functions might be lateralized in rats: An approach combining gene expression profiling and reversible inactivation. *Hippocampus*, **19**, 800-816.

Kohl, M.M., Shipton, O.A., Deacon, R.M., Rawlins, J.N., Deisseroth, K. & Paulsen, O. (2011) Hemisphere-specific optogenetic stimulation reveals left-right asymmetry of hippocampal plasticity. *Nat Neurosci*, **14**, 1413-1415.

Laurberg, S. (1979) Commissural and intrinsic connections of the rat hippocampus. *J Comp Neurol*, **184**, 685-708.

Laurberg, S. & Sorensen, K.E. (1981) Associational and commissural collaterals of neurons in the hippocampal formation (hilus fasciae dentatae and subfield CA3). *Brain Res*, **212**, 287-300.

Lein, E.S., Callaway, E.M., Albright, T.D. & Gage, F.H. (2005) Redefining the boundaries of the hippocampal CA2 subfield in the mouse using gene expression and 3-dimensional reconstruction. *J Comp Neurol*, **485**, 1-10.

Lein, E.S., Hawrylycz, M.J., Ao, N., Ayres, M., Bensinger, A., Bernard, A., Boe, A.F., Boguski, M.S., Brockway, K.S., Byrnes, E.J., Chen, L., Chen, L., Chen, T.M., Chin, M.C., Chong, J., Crook, B.E., Czaplinska, A., Dang, C.N., Datta, S., Dee, N.R., Desaki, A.L., Desta, T., Diep, E., Dolbeare, T.A., Donelan, M.J., Dong, H.W., Dougherty, J.G., Duncan, B.J., Ebbert, A.J., Eichele, G., Estin, L.K., Faber, C., Facer, B.A., Fields, R., Fischer, S.R., Fliss, T.P., Frensley, C., Gates, S.N., Glattfelder, K.J., Halverson, K.R., Hart, M.R., Hohmann, J.G., Howell, M.P., Jeung, D.P., Johnson, R.A., Karr, P.T., Kawal, R., Kidney, J.M., Knapik, R.H., Kuan, C.L., Lake, J.H., Laramee, A.R., Larsen, K.D., Lau, C., Lemon, T.A., Liang, A.J., Liu, Y., Luong, L.T., Michaels, J., Morgan, J.J., Morgan, R.J., Mortrud, M.T., Mosqueda, N.F., Ng, L.L., Ng, R., Orta, G.J., Overly, C.C., Pak, T.H., Parry, S.E., Pathak, S.D., Pearson, O.C., Puchalski, R.B., Riley, Z.L., Rockett, H.R., Rowland, S.A., Royall, J.J., Ruiz, M.J., Sarno, N.R., Schaffnit, K., Shapovalova, N.V., Sivisay, T., Slaughterbeck, C.R., Smith, S.C., Smith, K.A., Smith, B.I., Sodt, A.J., Stewart, N.N., Stumpf, K.R., Sunkin, S.M., Sutram, M., Tam, A., Teemer, C.D., Thaller, C., Thompson, C.L., Varnam, L.R., Visel, A., Whitlock, R.M., Wohnoutka, P.E., Wolkey, C.K., Wong, V.Y., Wood, M., Yaylaoglu, M.B., Young, R.C., Youngstrom, B.L., Yuan, X.F., Zhang, B., Zwingman, T.A. & Jones, A.R. (2007) Genome-wide atlas of gene expression in the adult mouse brain. *Nature*, **445**, 168-176.

Lein, E.S., Zhao, X. & Gage, F.H. (2004) Defining a molecular atlas of the hippocampus using DNA microarrays and high-throughput in situ hybridization. *J Neurosci*, **24**, 3879-3889.

Li, X.G., Somogyi, P., Ylinen, A. & Buzsaki, G. (1994) The hippocampal CA3 network: an in vivo intracellular labeling study. *J Comp Neurol*, **339**, 181-208.

Lister, J.P., Tonkiss, J., Blatt, G.J., Kemper, T.L., DeBassio, W.A., Galler, J.R. & Rosene, D.L. (2006) Asymmetry of neuron numbers in the hippocampal formation of prenatally malnourished and normally nourished rats: a stereological investigation. *Hippocampus*, **16**, 946-958.

Magloczky, Z., Acsady, L. & Freund, T.F. (1994) Principal cells are the postsynaptic targets of supramammillary afferents in the hippocampus of the rat. *Hippocampus*, **4**, 322-334.

Mercer, A., Trigg, H.L. & Thomson, A.M. (2007) Characterization of neurons in the CA2 subfield of the adult rat hippocampus. *J Neurosci*, **27**, 7329-7338.

Ochiishi, T., Saitoh, Y., Yukawa, A., Saji, M., Ren, Y., Shirao, T., Miyamoto, H., Nakata, H. & Sekino, Y. (1999) High level of adenosine A1 receptor-like immunoreactivity in the CA2/CA3a region of the adult rat hippocampus. *Neuroscience*, **93**, 955-967.

Ramón y Cajal, S. (1911) *Histologie du système nerveux de l'hommes et des vertébrés*, Maloine, Paris.

Schwerdtfeger, W.K. & Buhl, E. (1986) Various types of non-pyramidal hippocampal neurons project to the septum and contralateral hippocampus. *Brain Res*, **386**, 146-154.

Sekino, Y., Obata, K., Tanifuji, M., Mizuno, M. & Murayama, J. (1997) Delayed signal propagation via CA2 in rat hippocampal slices revealed by optical recording. *J Neurophysiol*, **78**, 1662-1668.

Shinohara, Y., Hirase, H., Watanabe, M., Itakura, M., Takahashi, M. & Shigemoto, R. (2008) Left-right asymmetry of the hippocampal synapses with differential subunit allocation of glutamate receptors. *Proc Natl Acad Sci U S A*, **105**, 19498-19503.

Sik, A., Cote, A. & Boldogkoi, Z. (2006) Selective spread of neurotropic herpesviruses in the rat hippocampus. *J Comp Neurol*, **496**, 229-243.

Soto, D., Coombs, I.D., Renzi, M., Zonouzi, M., Farrant, M. & Cull-Candy, S.G. (2009) Selective regulation of long-form calcium-permeable AMPA receptors by an atypical TARP, gamma-5. *Nat Neurosci*, **12**, 277-285.

Spring, S., Lerch, J.P., Wetzel, M.K., Evans, A.C. & Henkelman, R.M. (2010) Cerebral asymmetries in 12-week-old C57Bl/6J mice measured by magnetic resonance imaging. *Neuroimage*, **50**, 409-415.

Stanfield, B.B. & Cowan, W.M. (1984) An EM autoradiographic study of the hypothalamo-hippocampal projection. *Brain Res*, **309**, 299-307.

Swanson, L.W., Sawchenko, P.E. & Cowan, W.M. (1980) Evidence that the commissural, associational and septal projections of the regio inferior of the hippocampus arise from the same neurons. *Brain Res*, **197**, 207-212.

Swanson, L.W., Wyss, J.M. & Cowan, W.M. (1978) An autoradiographic study of the organization of intrahippocampal association pathways in the rat. *J Comp Neurol*, **181**, 681-715.

Tamamaki, N., Abe, K. & Nojyo, Y. (1988) Three-dimensional analysis of the whole axonal arbors originating from single CA2 pyramidal neurons in the rat hippocampus with the aid of a computer graphic technique. *Brain Res*, **452**, 255-272.

Tamamaki, N., Watanabe, K. & Nojyo, Y. (1984) A whole image of the hippocampal pyramidal neuron revealed by intracellular pressure-injection of horseradish peroxidase. *Brain Res*, **307**, 336-340.

Thompson, C.L., Pathak, S.D., Jeromin, A., Ng, L.L., MacPherson, C.R., Mortrud, M.T., Cusick, A., Riley, Z.L., Sunkin, S.M., Bernard, A., Puchalski, R.B., Gage, F.H., Jones, A.R., Bajic, V.B., Hawrylycz, M.J. & Lein, E.S. (2008) Genomic anatomy of the hippocampus. *Neuron*, **60**, 1010-1021.

Tomioka, R. & Rockland, K.S. (2006) Improved Golgi-like visualization in retrogradely projecting neurons after EGFP-adenovirus infection in adult rat and monkey. *J Histochem Cytochem*, **54**, 539-548.

Verstynen, T., Tierney, R., Urbanski, T. & Tang, A. (2001) Neonatal novelty exposure modulates hippocampal volumetric asymmetry in the rat. *Neuroreport*, **12**, 3019-3022.

Vertes, R.P. & McKenna, J.T. (2000) Collateral projections from the supramammillary nucleus to the medial septum and hippocampus. *Synapse*, **38**, 281-293.

West, J.R., Nornes, H.O., Barnes, C.L. & Bronfenbrenner, M. (1979) The cells of origin of the commissural afferents to the area dentata in the mouse. *Brain Res*, **160**, 203-215.

Williams, T.E., Meshul, C.K., Cherry, N.J., Tiffany, N.M., Eckenstein, F.P. & Woodward, W.R. (1996) Characterization and distribution of basic fibroblast growth factor-containing cells in the rat hippocampus. *J Comp Neurol*, **370**, 147-158.

Witter, M.P. & Amaral, D.G. (2004) Hippocampal Formation. In Paxinos, G. (ed.) *The Rat Nervous System*. Elsevier Academic Press, San Diego, pp. 635-704.

Wouterlood, F.G., Saldana, E. & Witter, M.P. (1990) Projection from the nucleus reuniens thalami to the hippocampal region: light and electron microscopic tracing study in the rat with the anterograde tracer Phaseolus vulgaris-leucoagglutinin. *J Comp Neurol*, **296**, 179-203.

Wyszynski, M., Lin, J., Rao, A., Nigh, E., Beggs, A.H., Craig, A.M. & Sheng, M. (1997) Competitive binding of alpha-actinin and calmodulin to the NMDA receptor. *Nature*, **385**, 439-442.

Zappone, C.A. & Sloviter, R.S. (2001) Commissurally projecting inhibitory interneurons of the rat hippocampal dentate gyrus: a colocalization study of neuronal markers and the retrograde tracer Fluoro-gold. *J Comp Neurol*, **441**, 324-344.

Zhao, M., Choi, Y.S., Obrietan, K. & Dudek, S.M. (2007) Synaptic plasticity (and the lack thereof) in hippocampal CA2 neurons. *J Neurosci*, **27**, 12025-12032.

## Figure Legends

### Figure 1

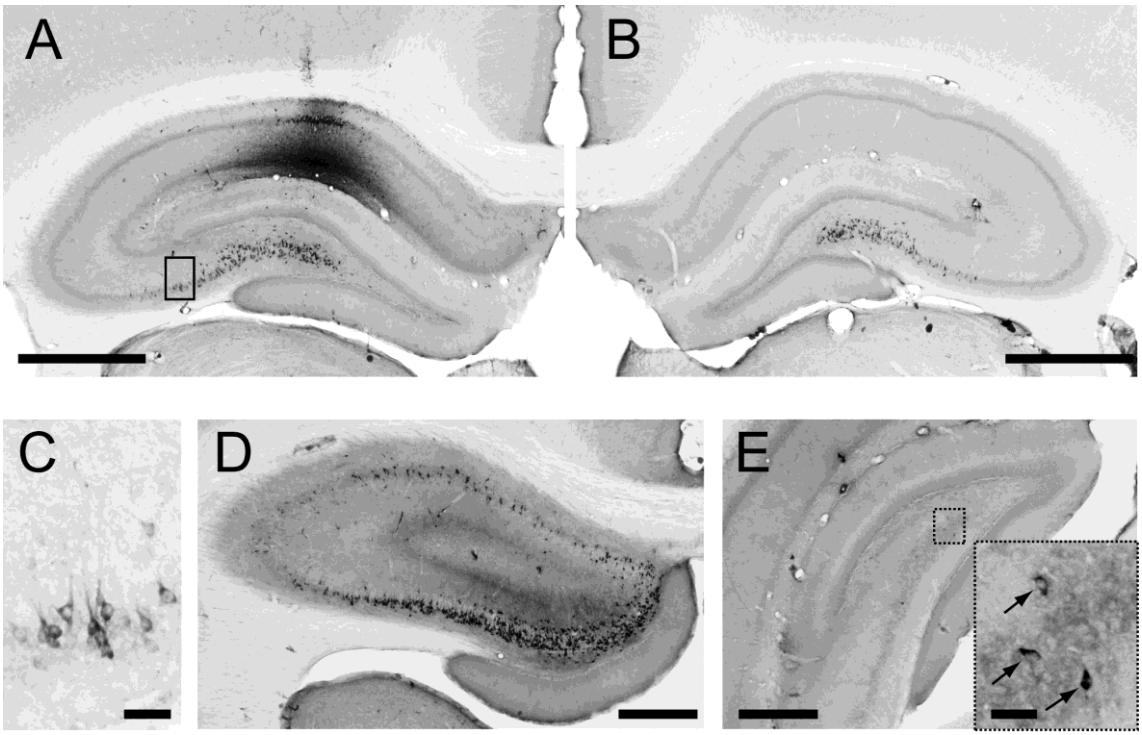


Retrograde tracing of CA3-CA1 connections using CTB. The sections are weakly counterstained with cresyl violet to visualize the cell body layer. **A.** The micrograph shows the CTB injection site in the dorsal CA1 *stratum radiatum*. **B.** Contralateral dorsal hippocampus of the same coronal section as A. In both A and B, CA3 neurons are retrogradely labeled. **C.** Magnification of the solid-line box in A. **D.** Ipsilateral anterior portion of the hippocampus of the same animal as A. **E.** Ipsilateral posterior portion of the hippocampus of the same animal as A. The posterior CA3 labeling is sparse, compared with the anterior CA3. Inset is a magnified view of the dotted box. Three neurons are labeled as indicated by arrows. Scale bar: A,B 1 mm; C,E (inset) 50 µm; D,E 500 µm.

**Figure 2**

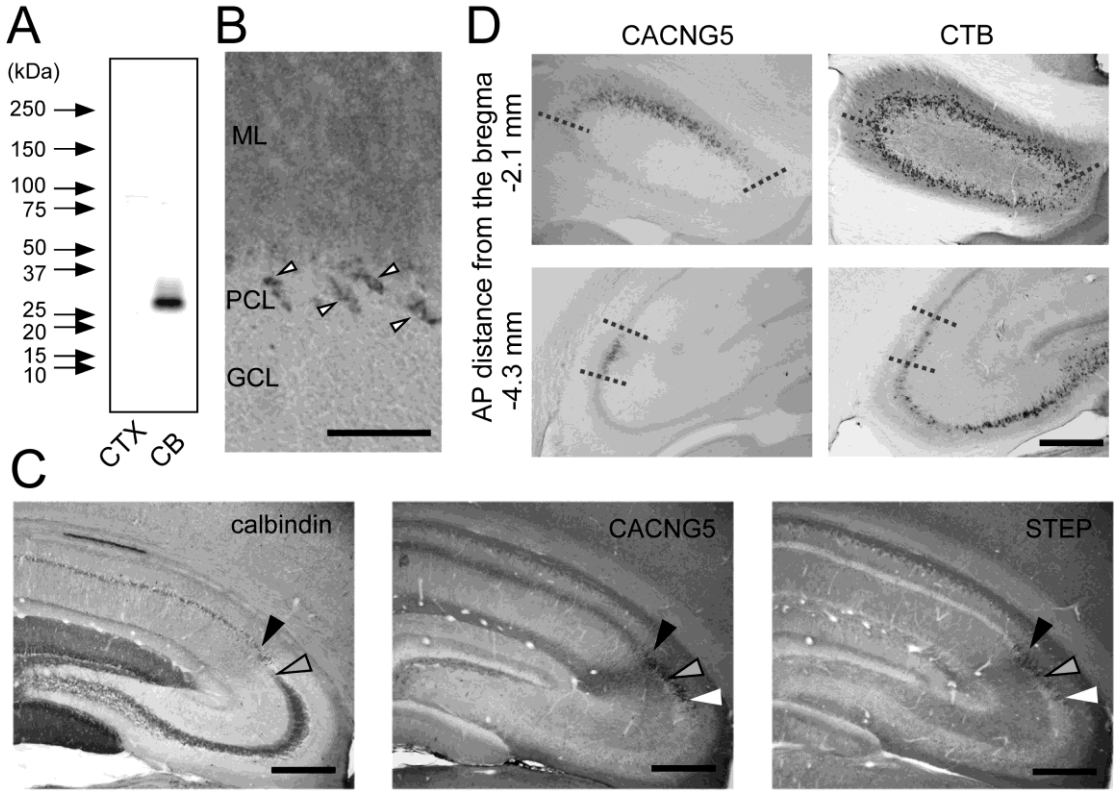


Visualization of CA2 by CACNG5 immunohistochemistry. **A.** Western blot analysis of mouse cerebral cortex (CTX, left) and cerebellum (CB, right) using the CACNG5 antibody. **B.** Immunohistochemistry of rat cerebellar cortex using the CACNG5 antibody shows localization of the immunoreaction to Bergmann glia (arrow). **C.** Immunohistochemitry for calbindin-D28k (left), CACNG5 (middle) and STEP (right) is shown for three consecutive dorsal hippocampal sections from a rat. Black and gray arrows indicate distal and proximal CA2 borders according to the classical definition of CA2 in calbindin-D28k staining. White arrows indicate molecularly defined CA2 borders by CACNG5 or STEP expression. **D.** Left panels show the immunohistochemical localization of CACNG5 in anterior (upper panel) and posterior (lower panel) coronal hippocampal sections. Right panels show CTB tracing results that correspond to similar areas as the left panels. Thick dotted lines show the limit of the CA2 region. Scale bar: B 100 µm; C,D 500 µm. ML: molecular layer; PC: Purkinje cell layer; GCL: granule cell layer; AP: anterior-posterior.

**Figure 3**

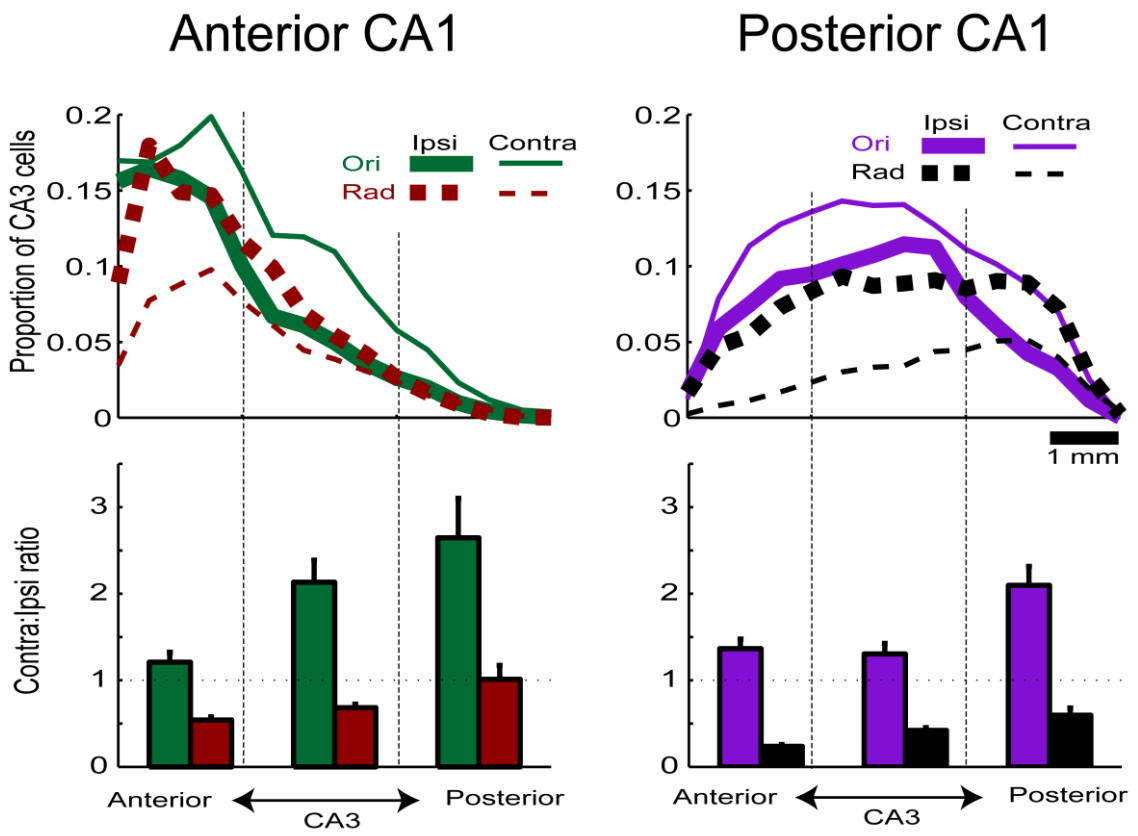


Topology of CA3-CA1 connections identified by retrograde tracing. Upper traces: Proportions of CA3 cells contributing to projections to various regions of CA1 are plotted. Contralateral projections are normalized to the respective ipsilateral projections. Lower traces: ratios of contralateral projections to ipsilateral CA3 projections to a given CA1 region are computed in three regions of CA3 separated by the anterior-posterior positions. Error bars are SEM.

**Figure 4**

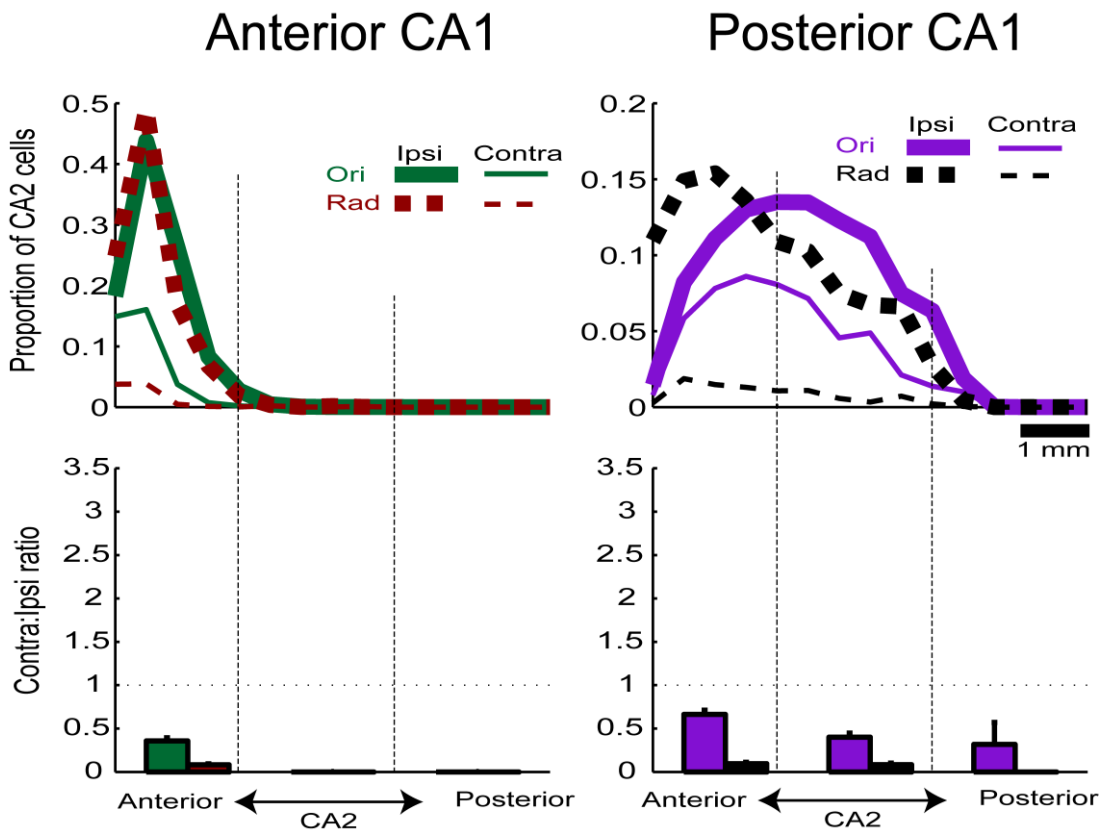


Topology of CA2-CA1 connections identified by retrograde tracing. The figure arrangements are similar to that of Figure 3.

**Figure 5**

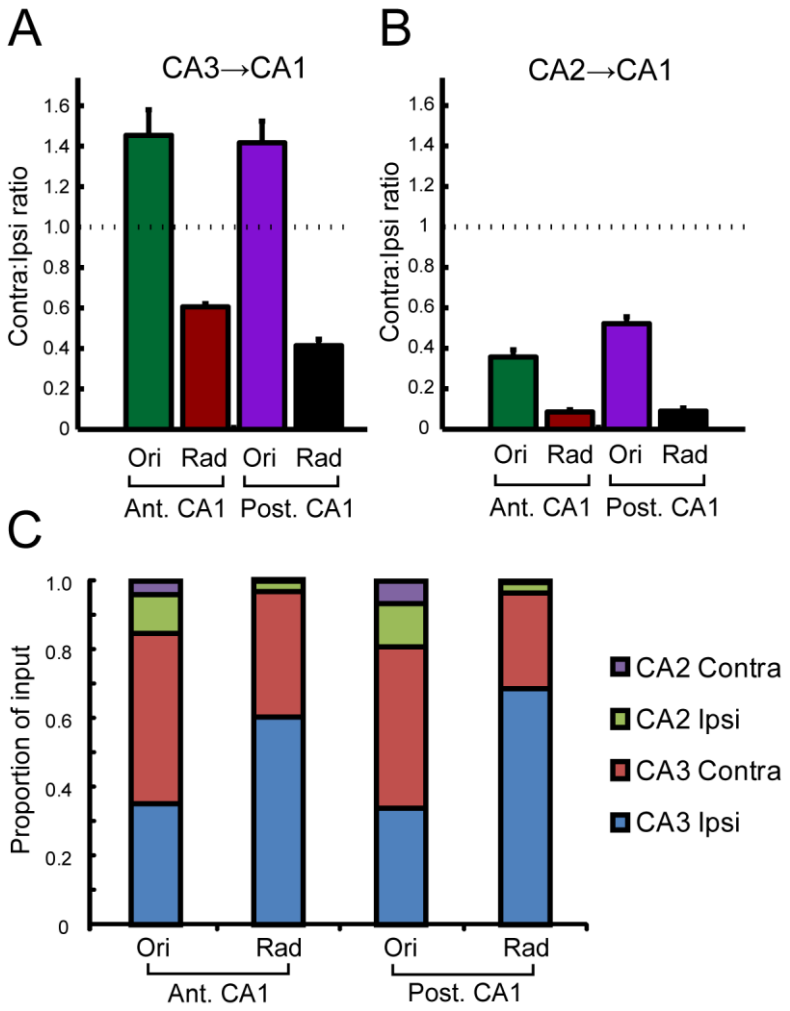


Overall ratios of ipsilateral and contralateral innervation to various CA1 areas.

**A.** Contra- vs. ipsirateral projection ratio of CA3 projections to different areas of CA1.

**B.** Contra- vs. ipsirateral projection ratio of CA2 projections to different areas of CA1.

**C.** Relative contributions of ipsi- and contralateral CA2 and CA3 projection to different areas of CA1.

**Figure 6**

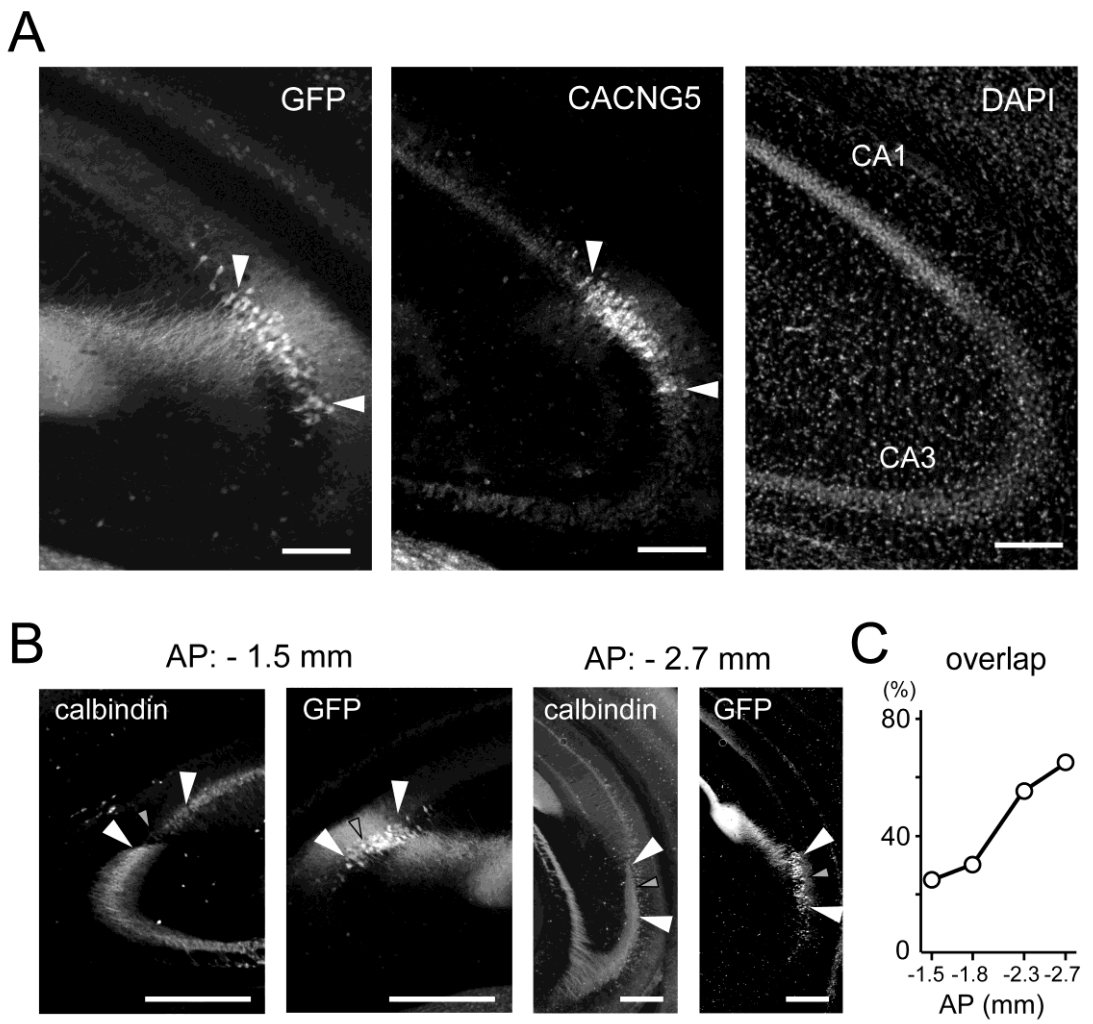


Immunohistological characterization of CACNG5-GFP transgenic mouse hippocampus. **A.** Cells in a restricted region between CA3 and CA1 express high levels of GFP. Double immunostaining of GFP (left) and CACNG5 (middle) reveals that the region with high CACNG5 expression (between the white arrowheads) maps well with the GFP positive cell population. The section is counterstained by DAPI for cell body layer location (right). **B.** The GFP expressing cells are localized in a small distal portion (~120 µm) of CA3a in addition to the CA2 area, as revealed by visualizing CA3 *stratum lucidum* by calbindin-D28k immunostaining. Large white arrowheads indicate the borders of the GFP expressing cell population. Small gray arrowheads indicate where the *stratum lucidum* disappears. **C.** Quantification of the proportion of CA3a in the

molecularly defined CA2 along the anterior-posterior (AP) axis. Scale bars: A 200 µm; B 500 µm.

## Figure 7

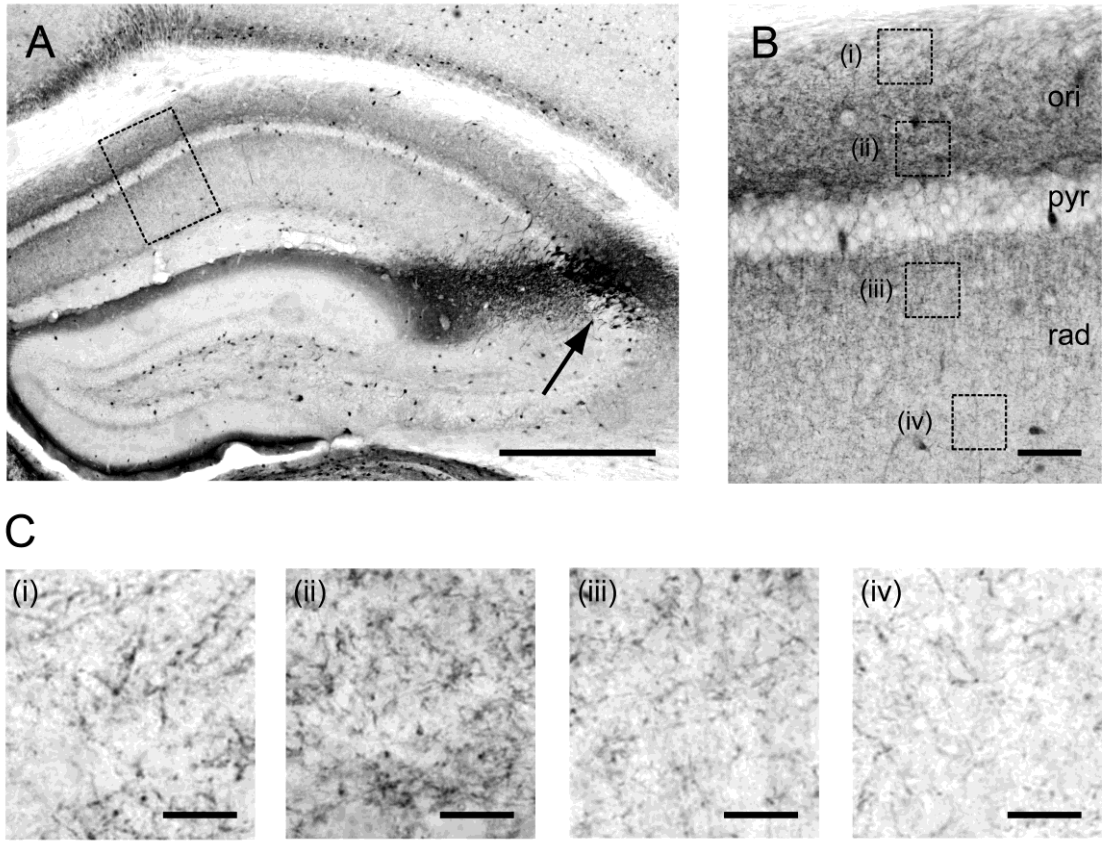


The axonal projection patterns of CA2 pyramidal cells are visualized by GFP immunohistochemistry in CACNG5-GFP transgenic mice. **A.** Immunohistochemistry for GFP expression shows intense labeling of CA2 pyramidal cells (arrow). **B.** Magnified view of the dotted area in A shows labeling of axon-like structures in the CA1 *stratum oriens* (ori) and *stratum radiatum* (rad), whereas the *stratum pyramidale* (pyr) is devoid of intense labeling. **C.** The dotted rectangles in B are further magnified to show that the labeling is stronger in the *stratum* oriens, in particular, the area closer to the *stratum pyramidale*. Scale bars: A 500 µm; B 50 µm; C(i)-(iv) 10 µm.

## Supplementary Figure 1

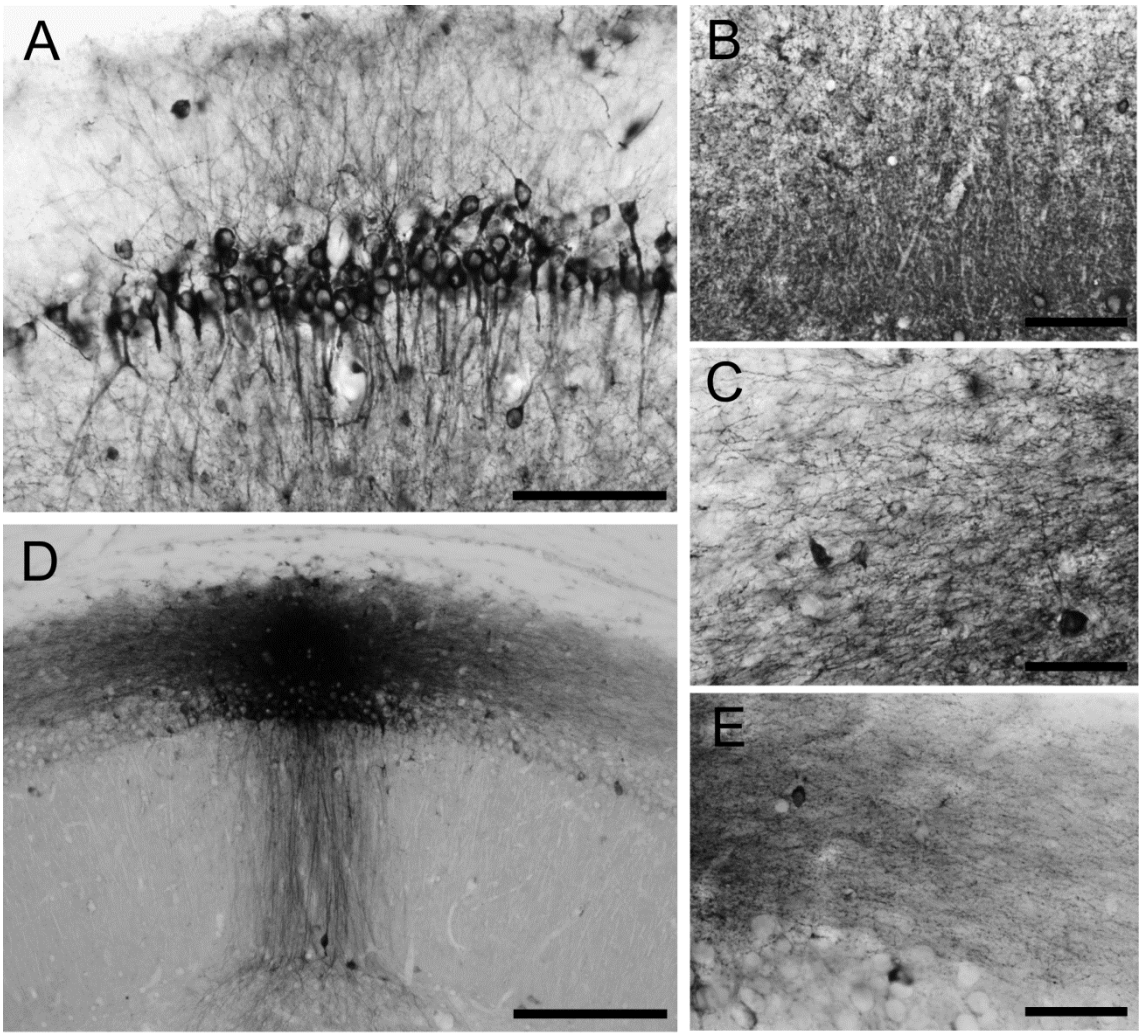


Spread of retrograde tracer. **A.** Magnified view around the *stratum pyramidale* of the tracer injection site displayed in Figure 1. The pyramidal cells are anterogradely labeled. The darkened appearance of the *stratum oriens* labeling in Figure 1 is a product of neuronal process labeling by the anterograde tracing which is limited to the injection site. **B.** Neuropil labeling near the center of the injection site of Figure 1. The labeling is too dense to discriminate individual fibers, possibly because of the residual tracers. **C.** Magnified view of the *stratum radiatum* approximately 250 μm away (towards CA2) from the injection site of Figure 1. Note that the labeling is predominantly axon-like fiber structures. **D.** Example of *stratum oriens* injection. Pyramidal layer seems to

function as a diffusion barrier and the labeling in the *stratum radiatum* is limited to the apical dendrites of anterogradely labeled CA1 pyramidal cells and some retrogradely labeled interneurons. **E.** Magnified view of the *stratum oriens*, approximately 200 µm away (towards the midline) from the injection site shown in D. Note that the labeling is predominantly axon-like fiber structures. Scale bars: A 100 µm; B,C,E 50 µm; D 200 µm.

## Tables and Table Legends

Table 1.

**Target coordinates of retrograde tracer injection in CA1**

| | AP (mm) | ML (mm) | DV (mm) |
|---|---|---|---|
| Anterior *stratum oriens* | -3.3 | 2.2 | 2.05 |
| Anterior *stratum radiatum* | -3.3 | 2.2 | 2.55 |
| Posterior *stratum oriens* | -5.4 | 5.0 | 2.55 |
| Posterior *stratum radiatum* | -5.4 | 5.0 | 3.05 |

Table 2.

**Relative contributions of CA3 and CA2 projections to CA1. The data are in %, mean ± s.e.m.**

| | Ipsi. CA3 | Contra. CA3 | Ipsi. CA2 | Contra. CA2 |
|---|---|---|---|---|
| Anterior *stratum oriens* | 35 ± 2 | 50 ± 2 | 11 ± 1 | 4 ± 1 |
| Anterior *stratum radiatum* | 60 ± 1 | 36 ± 1 | 3 ± 1 | 0 ± 1 |
| Posterior *stratum oriens* | 34 ± 2 | 47 ± 2 | 13 ± 1 | 7 ± 1 |
| Posterior *stratum radiatum* | 68 ± 2 | 28 ± 1 | 3 ± 1 | 0 ± 0 |